Antifouling coatings for optoelectronic tweezers

Aldrich N. K. Lau,[a] Aaron T. Ohta,[*b] Huan L. Phan,[a] Hsan-Yin Hsu,[c] Arash Jamshidi,[c] Pei-Yu Chiou[d] and Ming C. Wu[c]

Optoelectronic tweezers enables parallel manipulation of individual single cells using optical addressing and optically induced dielectrophoretic force. This provides a useful platform for performing a variety of biological functions, such as cell manipulation, cell sorting, and cell electroporation. However, in order to obtain more reliable cellular manipulation, especially of adherent mammalian cells, antifouling coatings need to be used to avoid non-specific cell adherence. Two antifouling coatings are discussed here, which can reduce the amount of non-specific adherence by as much as a factor of 30.

Introduction

Traditionally, biologists have studied cell behavior by observing the bulk response of a population of cells. However, single-cell studies yield insight into phenomena such as cell-cell interactions, cell signaling pathways, mutations or genetic damage among a population, or the differentiation of stem cells. Studying individual cells is greatly facilitated by the ability to manipulate single cells. Techniques for single-cell manipulation utilize a wide variety of forces, including mechanical,[1–3] magnetic,[4,5] hydrodynamic,[6–9] acoustic,[10,11] optical,[12,13] and electrokinetic[14–20] forces. However, it is difficult to perform parallel manipulation of many specific single cells using mechanical, hydrodynamic, or acoustic methods. Magnetic tweezers[5] can address specific single cells, but requires the use of magnetic tags. Label-free manipulation can be achieved using optical tweezers[21–23] or dielectrophoresis.[19,20]

Optical tweezers relies on the gradient force of a highly focused laser, trapping dielectric particles such as cells near the focal point, with forces typically in the hundreds of piconewtons.[21–23] Since its demonstration by Ashkin et al.,[21] optical tweezers has been used to manipulate cells and other bioparticles,[13,22,24,25] as well as to measure other cellular parameters such as motility forces.[12,26–28] However, in order to create a stable optical trap, high optical intensities of approximately 10^7 W/cm^2 or greater are required. Light of such a high intensity can induce adverse effects upon cells under manipulation.[29–31] In addition, although multiple optical tweezers traps can be created by using holographic techniques,[23] the overall manipulation area is still limited due to the focusing requirements, limiting the amount of cells that can be simultaneously manipulated. Plasmonic optical tweezers[32,33] have the potential to increase the trapping area, but sample heating is a concern for cell manipulation.

Dielectrophoresis (DEP) is the net force induced on a dipole due to a non-uniform electric field.[34] As with optical tweezers, the field gradient gives rise to the manipulation force. Microfabricated electrodes are typically used in order to create strong electric field gradients at length scales suitable for cellular manipulation. Suitably designed electrodes can be used for cell trapping, transportation, characterization, and sorting, with forces similar to that of optical tweezers.[14–20] However, it is difficult to isolate specific individual cells using fixed electrodes. Dynamic electrode cages have been demonstrated for reconfigurable cell manipulation;[35–37] however, if single-cell manipulation is required, electrode size must be carefully tailored to the size of the target cells.

Another tool exists that combines the advantages of optical manipulation (real-time reconfigurability and flexibility) with the advantages of dielectrophoresis (no photodamage, larger parallel-processing capabilities). This device relies upon the principle of optically induced dielectrophoresis, and is called optoelectronic tweezers (OET).[38] OET devices have been used for manipulating many types of particles, including polystyrene beads,[38–44] aqueous droplets,[45] semiconductor microdisks,[46] and nanowires,[47,48] as well as many mammalian cells, such as red blood cells,[40] white blood cells,[38,40,41] HeLa cells,[41,49] Jurkat cells,[41] and oocytes.[50] OET is capable of manipulating specific single cells in parallel, enabling single-cell studies. However, cell manipulation using OET is more challenging than the manipulation of polystyrene beads. Here, issues involved in the manipulation of mammalian cells are discussed, along with the implemented solutions. We then demonstrate OET manipulation for the patterning of cell arrays.

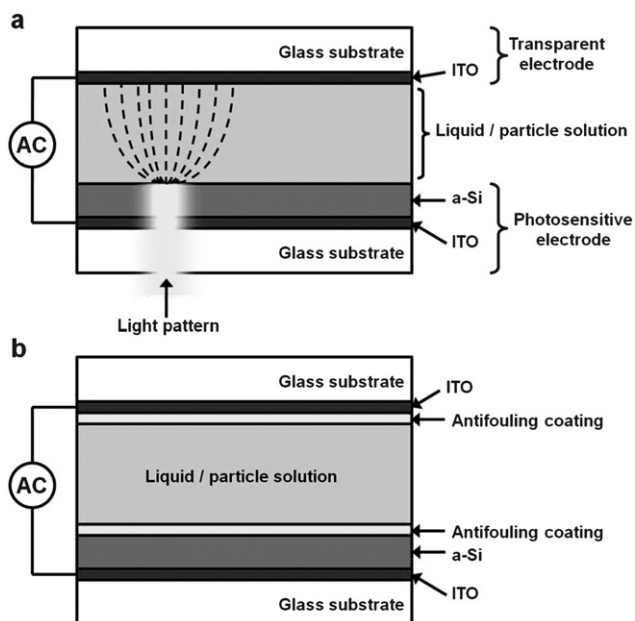## Optoelectronic tweezers (OET)

Although a few variations exist,[41,43,45,46] the standard optoelectronic tweezers device consists of two substrates: a glass slide coated with a layer (typically 100 to 200 nm) of indium tin oxide (ITO), and a separate ITO-coated glass slide that has an additional 1-μm-thick layer of amorphous silicon (a-Si) (Fig. 1a).[38] A microfluidic chamber with a height of approximately 100 μm is formed between the two glass slides. Aqueous solutions

[a] Applied Biosystems, Foster City, CA, 94404, USA. E-mail: lauan@appliedbiosystems.com
[b] Dept. of Electrical Engineering, University of Hawaii at Manoa, Honolulu, HI, 96822, USA. E-mail: aohta@hawaii.edu; Fax: +1-808-956-3427; Tel: +1-808-956-8196
[c] Dept. of Electrical Engineering & Computer Sciences, University of California, Berkeley, CA, 94720, USA
[d] Dept. Mechanical and Aerospace Engineering, University of California, Los Angeles, CA, 90095, USA

Fig. 1 Schematic cross-section of the optoelectronic tweezers (OET) device. (a) The OET device consists of two glass slides coated with a layer of indium tin oxide (ITO). The photosensitive electrode is coated with a layer of amorphous silicon (a-Si). Light patterns change the resistance of the a-Si layer, creating electric field gradients. The dashed lines represent electric field lines. (b) Schematic of the OET device, modified with antifouling coatings for adherent cell manipulation.

containing the cells under manipulation are added into this chamber. Electrical contacts on the ITO layers are used to bias the OET device, creating the electric field necessary for DEP force. Light patterns focused onto the OET device create optically induced DEP force, and control the position of cells in the OET device.

The light patterns induce DEP force by controlling the electric fields in the liquid solution inside the microfluidic chamber of the OET device. When the a-Si layer is illuminated by the optical pattern, its resistance is reduced by the photoconductive effect, making the applied bias drop across the liquid layer. In this manner, high electric fields are created in the liquid immediately above where the a-Si is illuminated. In the un-illuminated areas, the resistance of the a-Si is much larger, absorbing most of the applied bias. Thus, in the un-illuminated areas, low electric fields are present in the liquid. In this manner, electric field gradients are created that drive DEP force in the OET device in response to the light patterns.

OET operation is robust when using polystyrene beads, yeast cells, or other non-adhesive particles. However, the operation of OET using adherent mammalian cells is more complicated. A main factor that makes cellular manipulation using OET more challenging than the manipulation of polystyrene beads is the non-specific adhesion of cells to the OET surfaces. The non-specific adhesion of cells is a well-known issue in biomedical devices,[51] and is also a concern in OET devices. The fabrication of OET devices is simple enough to allow OET devices to be used as single-use, disposable devices, eliminating the cross-contamination concerns of unwanted cell adhesion. However, cellular adhesion, especially among mammalian cells that adhere to

surfaces in order to proliferate, is still significant during a single OET manipulation experiment. Many types of mammalian cells tend to adhere to charged hydrophilic surfaces, a condition which is present in the OET device, as the a-Si surface has a native oxide present at the a-Si/liquid interface. Adherent cells are capable of attaching to surfaces with forces on the order of nanonewtons, while OET produces forces in the tens to hundreds of piconewtons. Thus, it is necessary to passivate the surface of the OET device in order to prevent the undesirable adsorption of cells.

In order to avoid cell adhesion, the surfaces of the OET device need to be modified with adhesion-resistant passivation layers (Fig. 1b). Furthermore, the passivation layers must be non-conductive, to avoid shorting out the optically-defined virtual electrodes of the photosensitive electrode. At the same time, the non-conductive layers should be thin, in order to avoid any parasitic voltage drops across the passivation layers. Two types of surface treatments that fulfil these requirements have been used to prevent non-specific cell adhesion.

Antifouling coatings for optoelectronic tweezers

Bovine serum albumin (BSA) coating

One method to achieve an adhesion-resistant surface is to coat it with bovine serum albumin (BSA), a protein found in the bloodstream of bovines. Very thin layers of BSA protein can be created, making it suitable for use in the OET device.

Some proteins have a hydrophobic end and a hydrophilic end. Thus, to create an uncharged, hydrophilic coating, the hydrophobic end of the protein should be made to bond to the device surface. This creates an antifouling coating by resisting further non-specific protein adsorption. However, the a-Si surface of the OET device is hydrophilic due to the native oxide that forms over the a-Si. To create a hydrophobic layer, Teflon AF® is diluted with perfluoro-(2-perfluoro-n-butyl)tetrahydrofuran to a concentration of 0.2% (v/v). This solution is spin-coated on the OET device at 1500 rpm for 30 seconds, resulting in a Teflon layer that is approximately 50 nm thick. This non-conductive layer is thin enough to avoid adverse effects on OET operation. The Teflon-coated devices are cured at 150 °C on a hotplate for 20 minutes, and then immersed in a solution of 0.1% BSA in deionized (DI) water.

The hydrophobic ends of the protein bind to the Teflon, creating an antifouling protein layer. The devices are removed from the BSA solution after 30 minutes to 1 hour, and carefully dried with nitrogen gas.

Poly(ethylene glycol) (PEG) coating

The gold standard of non-fouling surface coatings for biomedical devices is poly(ethylene glycol) (PEG), a polymer hydrogel.[51] PEG is based on a repeating unit of ethylene glycol, and has the following structure: $HO–(–CH_2CH_2–O–)_n–H$. This surface has been shown to have an excellent resistance to protein and cell adsorption, reducing the amount of biofouling by more than 90%.[51] The model for the nonfouling properties of PEG is based on entropic repulsion and osmotic pressure; as the PEG hydrogel is hydrated, the PEG chain swells and excludes cells and proteins from the PEG surface.[52,53] In order to achieve a high-quality

nonfouling surface, a high surface density of grafted PEG chains is required. The PEG chains should be dense enough that the distance between grafted chains is approximately less than or equal to the radius of gyration of a hydrated PEG chain.[54]

To coat the photosensitive electrodes with PEG, the a-Si surface is first coated with a 10-nm-thick layer of SiO_2 using PECVD. The SiO_2 layer provides a surface that can be silanized to provide adhesion of the PEG polymer chains. Following the SiO_2 deposition, the a-Si electrodes are rinsed with ethanol, dried using nitrogen, and baked at 110 °C for 30 minutes in a convection oven. The a-Si chips then undergo a series of chemical washes to silanize the surface, enhancing PEG attachment. First, the devices are bathed in a 1:1:4 volume ratio of 29% NH_4OH, 30% H_2O_2, and DI water for 60 minutes, then rinsed with DI water. This is followed by another bath in a 1:1:4 volume ratio of 38% HCl, 30% H_2O_2, and DI water for 60 minutes. The chips are again rinsed with DI water, dried with nitrogen, and baked at 110 °C for 30 minutes in a convection oven to remove all moisture. A solid PEG-silane of 2-[methoxy(polyethyleneoxy)propyl]-trimethoxysilane (MW 5,000 obtained from Nektar or Laysan) is placed directly on the surface of the a-Si electrodes, covered with a microscope glass cover slide, and melted using a hotplate at 65 °C for 16 hours. The PEG-coated chips are then rinsed with plenty of DI water and annealed at 110 °C for 10 minutes in a convection oven.

The fabrication process for coating the ITO-coated glass electrodes with PEG is similar to the process for the photosensitive electrodes. First, the ITO electrodes are rinsed with copious amounts of DI water, methanol, acetone, methanol, and DI water, respectively, then dried using nitrogen. The ITO electrodes are then baked at 110 °C for 10 minutes in a convection oven. The ITO chips then undergo a chemical tretment to silanize the surface, enhancing PEG attachment. The ITO chips are bathed in a 1:1:4 volume ratio of 29% NH_4OH, 30% H_2O_2, and DI water for 60 minutes. Next, they are rinsed with DI water, dried with nitrogen, then baked at 110 °C for 10 minutes to remove all moisture. The solid PEG-silane is placed on the surface of the ITO electrodes, covered with a microscope glass cover slide, and melted using a hotplate at 65 °C for 16 hours. The PEG-coated chips are then rinsed with plenty of DI water, and annealed at 110 °C for 10 minutes in a convection oven.

Results and discussion

X-ray photoemission spectroscopy (XPS) measurements

The resistance to protein adsorption of the PEG-coated OET devices was verified by X-ray photoemission spectroscopy (XPS) measurements. The XPS measurements are performed at the Molecular Foundry facility of the Lawrence Berkeley National Laboratories, using a Physical Electronics PHI 5400 XPS tool, which was equipped with an aluminium X-ray source. The measurement area of each sample is approximately 0.5 mm × 0.5 mm.

A standard OET device and a PEGylated OET device were both exposed to a solution of 0.1% laminin protein. The XPS spectrum of the uncoated a-Si electrode shows the presence of oxygen, nitrogen, and carbon from the adsorbed proteins (Fig. 2a). The PEG-coated a-Si electrode also has oxygen and carbon present due to the PEG layer, but it lacks a nitrogen peak,
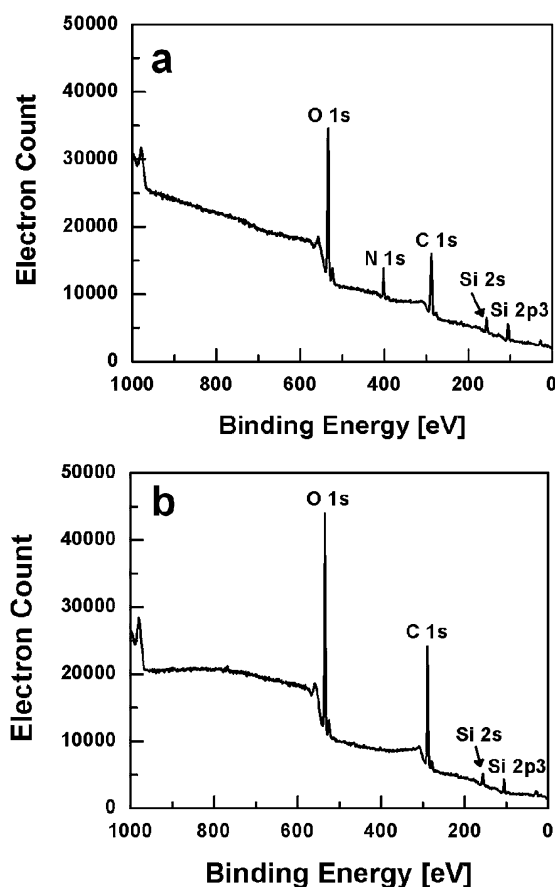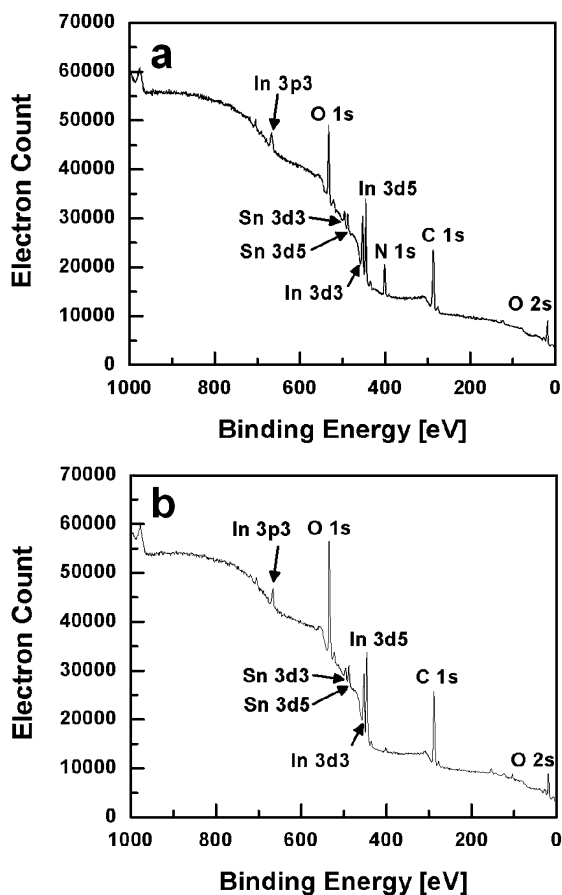
Fig. 2 XPS measurements of laminin adsorption on the a-Si electrode of an OET device. (a) Standard a-Si electrode. (b) PEG-coated a-Si electrode. The absence of an N 1s peak in this spectrum is an indicator of the resistance to protein adsorption.

indicating the absence of adsorbed laminin proteins (Fig. 2b). Silicon from the a-Si film is also present, suggesting the PEG layer is thin, as desired. The carbon/oxygen (C/O) ratio of the PEG-coated a-Si electrode is 1.63. An ideal PEG layer has a C/O ratio of 2; however, the C/O ratio of the measured device may be lower due to the presence of the SiO_2 layer.

The XPS spectrum of the ITO electrode shows similar results as the a-Si electrode. Again, the spectrum shows the presence of oxygen, nitrogen, and carbon from the adsorbed proteins (Fig. 3a). As expected, indium and tin are also present, due to the ITO film. The PEG-coated ITO electrode also has oxygen and carbon present due to the PEG layer, but it lacks a nitrogen peak, indicating the absence of adsorbed laminin proteins (Fig. 3b). The C/O ratio of the PEG-coated ITO electrode is 1.55, which is again lower than the ideal C/O ratio. However, the C/O ratio may be affected by the oxygen content of the ITO film.

Cell adhesion tests

In order to test the quality of the anti-adhesion coatings in a typical OET experimental procedure, adherent HeLa endothelial cells (a cervical cancer cell line) were used to quantify the prevalence of nonspecific cell adhesion. The HeLa cells, suspended in isotonic solution at a density of approximately
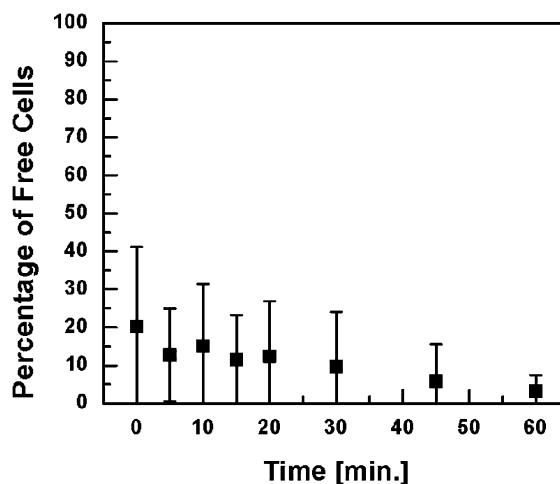
Fig. 4 Percentage of live HeLa cells that can be transported under OET manipulation in standard OET devices. Non-specific cell adhesion limits the reliability of OET manipulation of mammalian cells. The error bars indicate the standard deviation of the measurements.

OET manipulation on live adherent cells by 30 times compared to an uncoated OET device. Thus, the PEG coating is the most effective passivation layer to avoid non-specific cell adhesion in the OET device. In addition, the PEG-coated devices are more robust than the BSA-coated devices. Even after the devices were rinsed multiple times using DI water, no change in the amounts of free cells were measured. It is also noted that no significant change in cell velocities, corresponding to the OET force, was observed for BSA- and PEG-coated OET devices as compared to uncoated OET devices.

Cell patterning

The reliable OET manipulation of single cells on PEG-coated devices can be used to spatially arrange live cells in arbitrary

Fig. 3 XPS measurements of laminin adsorption on the ITO electrode of an OET device. (a) Standard ITO electrode. (b) PEG-coated ITO electrode. The absence of an N 1s peak in this spectrum is an indicator of the resistance to protein adsorption.

1×10^6 cells/mL, were introduced into the OET device in 20-μL aliquots. Attempts to move all cells within the microscope field-of-view (0.027 mm^2) were made using a 0.8-mW HeNe laser to actuate the OET device. Cells that exhibited movement as a result of the induced OET force were counted as "free" cells, while cells that did not have observable movement were counted as adhered cells. Five distinct fields-of-view were tested for each time point; at each time point, at least 30 cells were tested. The measurements were repeated on 5 different OET devices. On the standard OET devices, the initial percentage of free cells was only $20 \pm 21\%$, decreasing to $3 \pm 4\%$ after one hour (Fig. 4).

The same measurements of the percentage of free cells were repeated on 5 different BSA-coated OET devices (Fig. 5). The initial percentage of free cells was $88 \pm 7\%$, decreasing slightly to $82 \pm 15\%$ after one hour. However, when the BSA-coated OET devices were rinsed once using DI water, parts of the BSA coated were washed away, resulting in increased cell adhesion. In addition, certain areas of the OET surface had a high incidence of cell adhesion, evidenced by the large standard deviations.

Cell adhesion measurements were repeated on 5 different PEG-coated OET devices (Fig. 6). The initial percentage of free cells was $97 \pm 5\%$ on the PEG-coated OET devices. After one hour, $91 \pm 8\%$ of the cells remained responsive to OET manipulation. The PEG-coated OET devices increase the reliability of
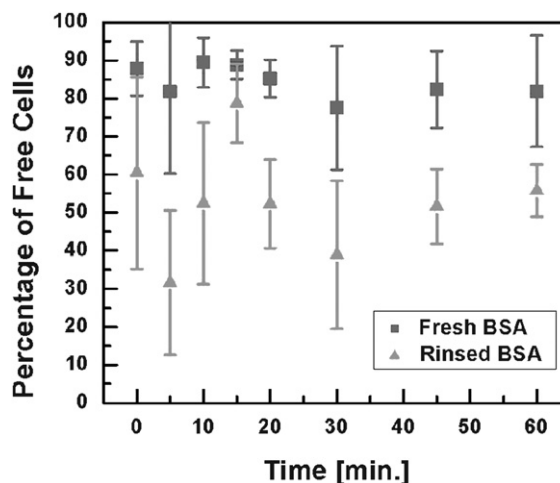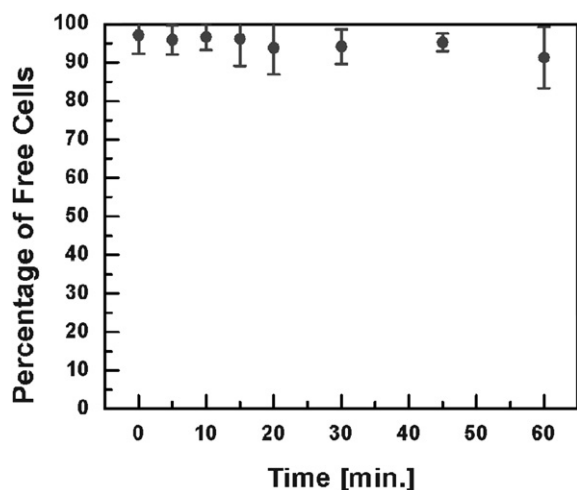

Fig. 5 Percentage of live HeLa cells that can be transported under OET manipulation in BSA-coated OET devices. Non-specific cell adhesion is greatly reduced by using this passivation technique. However, rinsing the devices results in increased non-specific adhesion. The error bars indicate the standard deviation of the measurements.

Fig. 6 Percentage of live HeLa cells that can be transported under OET manipulation in PEG-coated OET devices. Non-specific cell adhesion is reduced 30 times by this passivation technique. The error bars indicate the standard deviation of the measurements. The PEG coating provides the most robust coating, and the most reliable OET manipulation.

patterns. This type of manipulation is not possible on untreated OET devices, as non-specific cell adhesion is too prevalent.

Here, we use OET manipulation to assemble Jurkat cells into a cell array (Fig. 7). The optical manipulation patterns are generated using a 635-nm laser and a liquid-crystal SLM. The optical manipulation patterns are created under direct user control.

Furthermore, multiple cell types can be trapped and transported using OET manipulation. This is demonstrated with live fluorescent-labeled Jurkat cells and unlabeled HeLa cells (Fig. 8). Each cell type can be identified *via* fluorescent microscopy, and subsequently trapped and transported under OET manipulation.
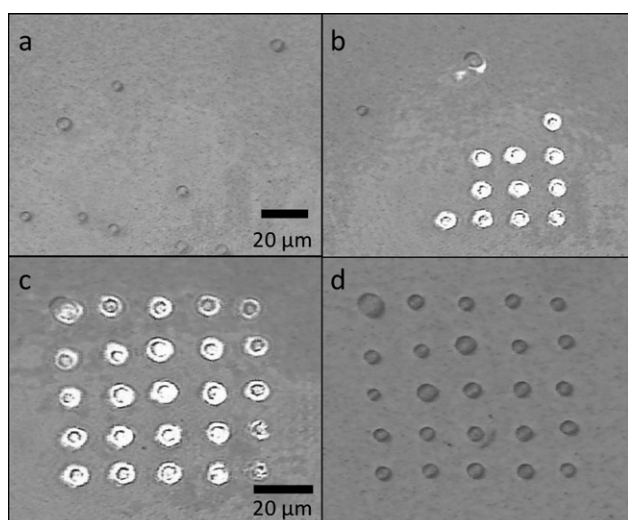
Fig. 7 Formation of an array of live Jurkat cells on a PEG-coated OET device. (a, b) The original randomly-distributed cells are trapped and transported using OET manipulation patterns. (c) A 5 × 5 individually-addressable cell array is formed. (d) The same array, with the OET manipulation pattern temporarily shut off for cell imaging clarity.
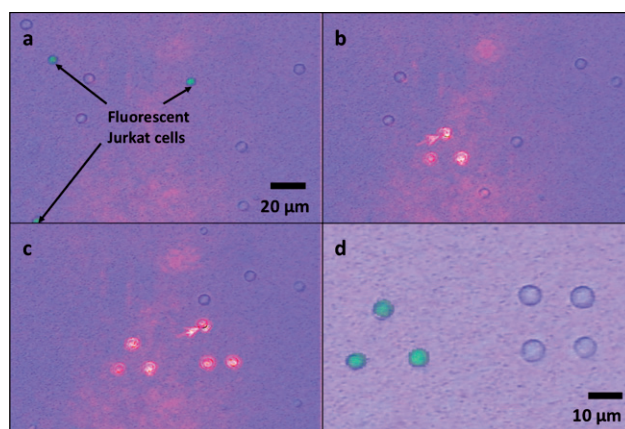
Fig. 8 OET spatial manipulation of multiple cell types. (a) The fluorescent-labeled Jurkat cells are distinguished from the unlabeled HeLa cells (composite image). (b) The Jurkat cells are arranged in a triangular pattern. (c) The HeLa cells are arranged in a square pattern. (d) Fluorescent imaging verifies that the cell types are segregated (composite image).

Thus, the original random distribution of the two cell types can be organized into segregated patterns for further single-cell study (Fig. 8d).

Conclusions

We have demonstrated and reviewed two methods of passivating the surfaces of the OET device. Treatment using BSA is a simpler process, but the protein layer is easily washed off, reducing its effectiveness. Grafting PEG polymer chains to the OET device provides a robust antifouling coating that reduces non-specific cell adhesion by more than 30 times. This enables the use of the OET device as a cell patterning tool, which has not been previously demonstrated due to the prevalence of non-specific adhesion of mammalian cells. OET devices coated with antifouling coatings will greatly improve the performance of OET for biological samples.

References

1 C. J. Kim, A. P. Pisano and R. S. Muller, *IEEE Journal of Microelectromechanical Systems*, 1992, **1**, 31–36.
2 C. G. Keller and R. T. Howe, *Tenth Annual IEEE International Workshop on Micro Electro Mechanical Systems (MEMS)*, 1997.
3 N. Chronis and L. P. Lee, *IEEE Journal of Microelectromechanical Systems*, 2005, **14**, 857–863.
4 D. W. Inglis, R. Riehn, R. H. Austin and J. C. Sturm, *Appl. Phys. Lett.*, 2004, **85**, 5093–5095.
5 H. Lee, A. M. Purdon and R. M. Westervelt, *Appl. Phys. Lett.*, 2004, **85**, 1063–1065.
6 A. Y. Fu, H. P. Chou, C. Spence, F. H. Arnold and S. R. Quake, *Anal. Chem.*, 2002, **74**, 2451–2457.
7 A. R. Wheeler, W. R. Throndset, R. J. Whelan, A. M. Leach, R. N. Zare, Y. H. Liao, K. Farrell, I. D. Manger and A. Daridon, *Anal. Chem.*, 2003, **75**, 3581–3586.
8 A. Wolff, I. R. Perch-Nielsen, U. D. Larsen, P. Friis, G. Goranovic, C. R. Poulsen, J. P. Kutter and P. Telleman, *Lab Chip*, 2003, **3**, 22–27.
9 D. Di Carlo, L. Y. Wu and L. P. Lee, *Lab Chip*, 2006, **6**, 1445–1449.
10 S. K. Chung and S. K. Cho, *Journal of Micromechanics and Microengineering*, 2008, **18**.
11 S. K. Chung and S. K. Cho, *Microfluidics and Nanofluidics*, 2009, **6**, 261–265.

12 B. Maier, M. Koomey and M. P. Sheetz, *Proceedings Of The National Academy Of Sciences Of The United States Of America*, 2004, **101**, 10961–10966.

13 L. Paterson, E. Papagiakoumou, G. Milne, V. Garces-Chavez, S. A. Tatarkova, W. Sibbett, F. J. Gunn-Moore, P. E. Bryant, A. C. Riches and K. Dholakia, *Appl. Phys. Lett.*, 2005, **87**.

14 P. R. C. Gascoyne, X.-B. Wang, Y. Huang and F. F. Becker, *IEEE Transactions on Industry Applications*, 1997, **33**, 670–678.

15 J. Cheng, E. L. Sheldon, L. Wu, M. J. Heller and J. P. O'Connell, *Anal. Chem.*, 1998, **70**, 2321–2326.

16 Y. Huang, J. Yang, X. B. Wang, F. F. Becker and P. R. C. Gascoyne, *Journal of Hematotherapy & Stem Cell Research*, 1999, **8**, 481–490.

17 Y. Huang, J. M. Yang, P. J. Hopkins, S. Kassegne, M. Tirado, A. H. Forster and H. Reese, *Biomedical Microdevices*, 2003, **5**, 217–225.

18 R. Pethig, M. S. Talary and R. S. Lee, *IEEE Engineering in Medicine and Biology Magazine*, 2003, **22**, 43–50.

19 P. R. C. Gascoyne and J. V. Vykoukal, *Proceedings of the IEEE*, 2004, **92**, 22–42.

20 J. Voldman, *Annual Review of Biomedical Engineering*, 2006, **8**, 425–454.

21 A. Ashkin, J. M. Dziedzic, J. E. Bjorkholm and S. Chu, *Opt. Lett.*, 1986, **11**, 288–290.

22 A. Ashkin, J. M. Dziedzic and T. Yamane, *Nature*, 1987, **330**, 769–771.

23 D. G. Grier, *Nature*, 2003, **424**, 810–816.

24 A. Ashkin and J. M. Dziedzic, *Science*, 1987, **235**, 1517–1520.

25 R. W. Applegate Jr., J. Squier, T. Vestad, J. Oakey and D. W. M. Marr, *Optics Express*, 2004, **12**, 4390–4398.

26 N. Mishima, T. Kaneta and T. Imasaka, *Anal. Chem.*, 1998, **70**, 3513–3515.

27 A. D. Mehta, M. Rief, J. A. Spudich, D. A. Smith and R. M. Simmons, *Science*, 1999, **283**, 1689–1695.

28 T. Kaneta, N. Mishima and T. Imasaka, *Anal. Chem.*, 2000, **72**, 2414–2417.

29 K. Konig, H. Liang, M. W. Berns and B. J. Tromberg, *Opt. Lett.*, 1996, **21**, 1090–1092.

30 S. K. Mohanty, A. Rapp, S. Monajembashi, P. K. Gupta and K. O. Greulich, *Radiat. Res.*, 2002, **157**, 378–385.

31 K. C. Neuman, E. H. Chadd, G. F. Liou, K. Bergman and S. M. Block, *Biophys. J.*, 1999, **77**, 2856–2863.

32 A. N. Grigorenko, N. W. Roberts, M. R. Dickinson and Y. Zhang, *Nat. Photonics*, 2008, **2**, 365–370.

33 X. Miao and L. Y. Lin, *IEEE J. Sel. Top. Quantum Electron.*, 2007, **13**, 1655–1662.

34 H. A. Pohl, *Journal of Applied Physics*, 1958, **29**, 1182–1188.

35 N. Manaresi, A. Romani, G. Medoro, L. Altomare, A. Leonardi, M. Tartagni and R. Guerrieri, *IEEE Journal of Solid-State Circuits*, 2003, **38**, 2297–2305.

36 G. Medoro, N. Manaresi, A. Leonardi, L. Altomare, M. Tartagni and R. Guerrieri, *IEEE Sensors Journal*, 2003, **3**, 317–325.

37 A. B. Fuchs, A. Romani, D. Freida, G. Medoro, M. Abonnenc, L. Altomare, I. Chartier, D. Guergour, C. Villiers, P. N. Marche, M. Tartagni, R. Guerrieri, F. Chatelain and N. Manaresi, *Lab Chip*, 2006, **6**, 121–126.

38 P. Y. Chiou, A. T. Ohta and M. C. Wu, *Nature*, 2005, **436**, 370–372.

39 Y.-S. Lu, Y.-P. Huang, J. A. Yeh, C. Lee and Y.-H. Chang, *Optical and Quantum Electronics*, 2005, **37**, 1385–1395.

40 A. T. Ohta, P. Y. Chiou, T. H. Han, J. C. Liao, U. Bhardwaj, E. R. B. McCabe, F. Yu, R. Sun and M. C. Wu, *IEEE Journal of Microelectromechanical Systems*, 2007, **16**, 491–499.

41 A. T. Ohta, P.-Y. Chiou, H. L. Phan, S. W. Sherwood, J. M. Yang, A. N. K. Lau, H.-Y. Hsu, A. Jamshidi and M. C. Wu, *IEEE J. Sel. Top. Quantum Electron.*, 2007, **13**, 235–243.

42 S. L. Neale, M. Mazilu, J. I. B. Wilson, K. Dholakia and T. F. Krauss, *Optics Express*, 2007, **15**, 12619–12626.

43 H. Hwang, Y. Oh, J. J. Kim, W. Choi, J. K. Park, S. H. Kim and J. Jang, *Applied Physics Letters*, 2008, **92**, 3.

44 J. K. Valley, A. Jamshidi, A. T. Ohta, H.-Y. Hsu and M. C. Wu, *IEEE Journal of Microelectromechanical Systems*, 2008, **17**, 342–350.

45 S. Park, C. Pan, T.-H. Wu, C. Kloss, S. Kalim, C. E. Callahan, M. Teitell and E. P. Y. Chiou, *Appl. Phys. Lett.*, 2008, **92**, 151101–151103.

46 M.-C. Tien, A. T. Ohta, K. Yu, S. L. Neale and M. C. Wu, *Applied Physics A: Materials Science & Processing*, 2009.

47 A. Jamshidi, P. J. Pauzauskie, P. J. Schuck, A. T. Ohta, P. Y. Chiou, J. Chou, P. D. Yang and M. C. Wu, *Nat. Photonics*, 2008, **2**, 85–89.

48 A. T. Ohta, S. L. Neale, H. Y. Hsu, J. K. Valley and M. C. Wu, *IEEE/LEOS International Conference on Optical MEMS*, 2008.

49 J. K. Valley, S. Neale, H. Y. Hsu, A. T. Ohta, A. Jamshidi and M. C. Wu, *Lab Chip*, 2009.

50 H. Hwang, D.-H. Lee, W. Choi and J.-K. Park, *Biomicrofluidics*, 2009, **3**, 014103–014110.

51 P. Kingshott and H. J. Griesser, *Current Opinion In Solid State & Materials Science*, 1999, **4**, 403–412.

52 I. Szleifer, *Biophys. J.*, 1997, **72**, 595–612.

53 R. L. C. Wang, H. J. Kreuzer and M. Grunze, *J. Phys. Chem. B*, 1997, **101**, 9767–9773.

54 S. J. Sofia, V. Premnath and E. W. Merrill, *Macromolecules*, 1998, **31**, 5059–5070.